

Nuclear Composition of Magnetized GRB Jets

Sanshiro SHIBATA¹ and Nozomu TOMINAGA^{1,2}

¹*Department of physics, Konan University, 8-9-1 Okamoto, Kobe, Hyogo 658-8501, Japan*

²*Kavli Institute for the Physics and Mathematics of the Universe, University of Tokyo, 5-1-5 Kashiwanoha, Kashiwa, Chiba 277-8583, Japan*

E-mail: d1221001@center.konan-u.ac.jp

(Received ; accepted)

Abstract

We investigate the fraction of metal nuclei in the relativistic jets of gamma-ray bursts associated with core-collapse supernovae. We simulate the fallback in jet-induced explosions with two-dimensional relativistic hydrodynamics calculations and the jet acceleration with steady, radial, relativistic magnetohydrodynamics calculations, and derive detail nuclear composition of the jet by postprocessing calculation. We found that if the temperature at the jet launch site is above $4.7 \times 10^9 \text{K}$, quasi-statistical equilibrium (QSE) is established and heavy nuclei are dissociated to light particles such as ^4He during the acceleration of the jets. The criterion for the survival of metal nuclei is written in terms of the isotropic jet luminosity as $L_j^{\text{iso}} \lesssim 3.9 \times 10^{50} (R_i/10^7 \text{cm})^2 (1 + \sigma_i) \text{ erg s}^{-1}$, where R_i and σ_i are the initial radius of the jets and the initial magnetization parameter, respectively. If the jet is initially dominated by radiation field (i.e., $\sigma_i \ll 1$) and the isotropic luminosity is relatively high ($L_j^{\text{iso}} \gtrsim 4 \times 10^{52} \text{ ergs}^{-1}$), the metal nuclei cannot survive in the jet. On the other hand, if the jet is mainly accelerated by magnetic field (i.e., $\sigma_i \gg 1$), metal nuclei initially contained in the jet can survive without serious dissociation even for the case of high luminosity jet. If the jet contains metal nuclei, the dominant nuclei are ^{28}Si , ^{16}O , and ^{32}S and the mean mass number can be $\langle A \rangle \sim 25$.

Key words: gamma-ray burst: general — magnetohydrodynamics (MHD) — nuclear reactions, nucleosynthesis, abundances

1. INTRODUCTION

Gamma-ray bursts (GRBs) are one of the most energetic phenomena in the universe. They radiate enormous energies of the order of 10^{51} ergs mainly in the form of gamma-rays with the short duration, typically of ~ 10 s. Although the detailed radiation mechanism of gamma-rays is under debate, the radiation is thought to be originated from the ultra-relativistic jets with $\Gamma \gtrsim 100$, where Γ is the Lorentz factor of the jets (e.g., Mészáros 2006). Furthermore, it is known that GRBs with duration longer than 2 s, called long GRBs, are associated with highly energetic type Ic supernovae (e.g., Iwamoto et al. 1998). This implies that the relativistic jets are launched at deep inside of massive progenitor stars after the onset of the core-collapse.

Nuclear composition of GRB jet have been studied by several authors. Pruet et al. (2002), Lemoine (2002) and Beloborodov (2003) investigated within the framework of the standard fireball model (e.g., Mészáros 2006), assuming that GRB jet initially consists of free nucleons. The nucleons can recombine into deuterium and/or α particles as the jet expands and cools but metal nuclei heavier than carbon can not be produced. Thus, they conclude that the GRB jet consists only of light nuclei.

However, there is a caveat that the initial composition of the jet is not necessarily dominated by the free nucleons because the mechanism to launch a well-collimated

relativistic jet is not specified. The proposed mechanisms include neutrino annihilation (e.g., Woosley 1993; MacFadyen & Woosley 1999) and magnetic field (e.g., Blandford & Znajek 1977; Brown et al. 2000; McKinney 2006). In fact, some observations of GRBs suggest that their relativistic jets were initially dominated by the magnetic field energy flux (e.g., Zhang & Pe’er 2009; Guiriec et al. 2011). When the relativistic jets are launched by the magnetic field, the jets could involve heavy nuclei such as ^{56}Ni (Fujimoto et al. 2008) and thus the nuclear composition of the jets may be different from the one that is derived within the framework of standard fireball model.

Horiuchi et al. (2012) investigated survival of metal nuclei in relativistic jets. They analytically estimated the conditions to survive photodisintegration and spallation at the base of the jets, in the accelerating jets, and at the emission region of GRB. They argued that the nuclei can avoid the destructions for a range of jet parameters. For examples, the metal nuclei can survive at the base of the jet if the radius of the central engine is greater than $\sim 10^8$ cm or if the radiation luminosity is less than $\sim 10^{48}$ erg/s. They also investigated the possibility for entrainment of metal nuclei from stellar material during the jet propagation in the progenitor star and suggested that the entrainment is possible depending on the model parameters. However, they did not calculate detail nuclear reactions and did not present final nuclear compositions.

In this paper, we calculate non-equilibrium nuclear re-

actions during the fallback and jet acceleration, based on the thermal histories derived by the relativistic hydrodynamics calculations and the steady, radial, relativistic magnetohydrodynamics calculation. Then we present the criterion for the metal nuclei to survive without serious dissociation. For the initial composition, we assume that the GRB jet is initially made from falling matter during a relativistic jet-induced explosion. We adopt Wolf-Rayet stars proposed to be progenitors of GRB-SN and circumstantially treat the jet acceleration by thermal and/or magnetic pressure gradient and nucleosynthesis in relativistic jets.

This paper is organized as follows. In Section 2, we describe the method and the model of GRB jet. In Section 3, we present fallback in jet-induced explosions, hydrodynamic properties of the accelerating jet, and the final nuclear composition of the jet. The conclusion is presented in Section 4. Finally, the discussions are presented in Section 5.

2. METHOD & MODEL

2.1. Method

We calculate the nuclear composition of magnetized GRB jets with following two steps: (1) We follow fallback in a relativistic jet-induced explosion with a two-dimensional relativistic hydrodynamics calculation in order to derive the initial composition of jets. (2) We follow the acceleration of magnetized GRB jets after the launch of jets with a steady, radial, relativistic magnetohydrodynamics calculation, assuming an interaction between the jet and stellar mantle does not influence on the acceleration of the GRB outflow.

According to thermodynamical histories during the fallback and acceleration, nuclear reactions are calculated as a postprocessing (e.g., Hix & Thielemann 1996; Hix & Thielemann 1999). The nuclear reaction network includes 281 isotopes up to ^{79}Br . Here, we adopt an equation of state for relativistic particles, $p = e_{\text{int}}/3$, which means $\gamma_a = 4/3$ where γ_a is the adiabatic index, and assume that the internal energy is dominated by contribution from photons and e^\pm pairs. Temperature T is derived by following equation (e.g., Freiburghaus et al. 1999):

$$e_{\text{int}} = aT^4 \left(1 + \frac{7}{4} \frac{T_9^2}{T_9^2 + 5.3} \right), \quad (1)$$

where $a = 7.57 \times 10^{-15} \text{ erg cm}^{-3} \text{ K}^{-4}$ is the radiation constant and $T_9 = T/(10^9 \text{ K})$. We note that the non-relativistic gas pressure is negligible compared with radiation pressure because of the high entropy.

2.1.1. Fallback in relativistic jet-induced explosions

In jet-induced explosions, a considerable fallback takes place along the equatorial plane (e.g., Maeda & Nomoto 2003) and thus an interaction between the jets and cocoon and the stellar mantle determines which mass elements fallback to a central remnant. Therefore, a numerical simulation is required to correctly treat fallback in explosions with relativistic jets. Hence, we calculate relativistic jet-induced explosions of C+O stars with the use

of a two-dimensional relativistic Eulerian hydrodynamic code with the Newtonian self-gravity (Tominaga et al. 2007; Tominaga 2009).

Since the GRB jets consist of the falling matter, the initial composition of the outflow is set to be an integration of falling matter. However, as the freefall time of the matter at the inner boundary is short ($< 0.1 \text{ s}$), materials, that fall through the inner boundary well before the initiation of the jet injection, are likely to have been accreted to the central remnant before the jet injection and not to be re-ejected as the relativistic jets. Therefore, in this paper, only the matter falling after the initiation of the jet injection are assumed to be re-ejected and integrated as the initial composition of the outflow.

As the material falls, the temperature increases and nucleosynthesis may take place. Nucleosynthesis during the infall from the presupernova location to $r = R_i$ is calculated with a thermodynamical history taking into account heating due to the infall and cooling due to the Urca process (Bisnovatyi-Kogan 2002).

2.1.2. Steady relativistic magnetized outflow

We treat a GRB jet as a steady, radial, magnetized outflow with efficient magnetic dissipation. We assume that magnetic fields in the outflow are dominated by a toroidal component and that the field efficiently dissipates via magnetic reconnection as the outflow expands. Such efficient dissipation of magnetic fields creates strong magnetic pressure gradient which enables a direct conversion of magnetic field energy into kinetic energy (Drenkhahn 2002; Drenkhahn & Spruit 2002). We neglect gravitational force because the gravitational energy is small compared with the radiation energy or magnetic field energy in the models considered here.

The mass, momentum, and energy conservation equations for the steady, radial outflow with a toroidal magnetic field are described as follows (e.g. Lyutikov & Blandford 2003):

$$\frac{1}{r^2} \frac{\partial}{\partial r} (r^2 \rho \Gamma v) = 0, \quad (2)$$

$$\frac{1}{r^2} \frac{\partial}{\partial r} \left[r^2 \left\{ (w + b^2) \Gamma^2 v^2 + \frac{b^2}{2} \right\} \right] + \frac{\partial p}{\partial r} = 0, \quad (3)$$

$$\frac{1}{r^2} \frac{\partial}{\partial r} (r^2 (w + b^2) \Gamma^2 v) = 0, \quad (4)$$

where r , ρ , Γ , v , p , w , and b are distance from the center, proper mass density, outflow Lorentz factor, outflow velocity, pressure, enthalpy, and toroidal component of the magnetic four-vector, respectively. The enthalpy is defined by $w = \rho + e_{\text{int}} + p$ where e_{int} is the internal energy. Here we adopt the unit system in which the speed of light is unity.

We employ a following evolution equation for the magnetic field which includes dissipation of non-axisymmetric magnetic field produced by inclined rotator (Drenkhahn 2002):

$$\frac{\partial}{\partial r} (r b \Gamma v) = -\frac{r \Gamma b}{\tau_{\text{dis}}}, \quad (5)$$

where τ_{dis} is the dissipation time scale derived as follows:

$$\tau_{\text{dis}} = \frac{2\pi\Gamma^2}{\epsilon\Omega} \sqrt{1 + u_A^{-2}}, \quad (6)$$

where $u_A = b/\sqrt{w}$ is Alfvén four-velocity, Ω is an angular frequency of central object, and ϵ is a dimensionless factor.

From Equation (2)-(6), the evolution of the Lorentz factor can be written as

$$\frac{\partial\Gamma}{\partial r} = \frac{\gamma_a v^2 \Gamma^3}{(\Gamma^2 - \Gamma_f^2)(w - \gamma_a p)} \left\{ \frac{2p}{r} + \frac{(2 - \gamma_a)b^2}{\gamma_a v \tau_{\text{dis}}} \right\}, \quad (7)$$

where Γ_f is a Lorentz factor corresponding to phase velocity of a fast magnetosonic wave and can be expressed as (e.g., Lyutikov & Blandford 2003)

$$\Gamma_f = \sqrt{\frac{\gamma_a p + b^2}{w + b^2}}. \quad (8)$$

Equation (7) indicates that the flow is accelerated only when $\Gamma > \Gamma_f$ and the acceleration of the flow is infinity when $\Gamma = \Gamma_f$. These behaviors of the flow is due to the absence of the gravity in the above formulation. Thus, although the magnetic field possesses a part of the total energy, we assume that the flow is accelerated as if there is no magnetic field and the magnetization parameter defined by $\sigma \equiv b^2/w$ is constant until Γ reaches $2\Gamma_f$. Then, the flow is accelerated with Equation (7) at $\Gamma < \Gamma_f$.

2.2. Model

We parameterize the GRB outflow with six parameters: isotropic energy deposition rate L_j^{iso} , initial radius of the outflow R_i , initial Lorentz factor Γ_i , maximum Lorentz factor Γ_{max} , angular frequency of central object (including dimensionless factor) $\epsilon\Omega$, and initial magnetization parameter $\sigma_i = b_i^2/w_i$, where b_i and w_i is the initial toroidal component of the magnetic four-vector and the initial enthalpy, respectively.

In this paper, we investigate the dependence of final nuclear composition on L_j^{iso} , R_i , and σ_i for the C+O star models with metallicity $Z = 0$ and 0.02. We adopt progenitor stars constructed from C+O cores of $40M_\odot$ stars with $Z = 0$ and $Z = 0.02$ (Umeda & Nomoto 2005) by attaching C+O envelopes in hydrostatic and thermal equilibrium. The envelope connects to the core structures continuously and smoothly in the first order differentials (e.g., Saio et al. 1988) and extends down to a density $\rho = 10^{-10} \text{ g cm}^{-3}$.

The density at the O layer is one order of magnitude lower in the model with $Z = 0.02$ than in the model with $Z = 0$. The O layer can be divided into two layers according to the abundance of C and Mg, O+Mg and O+C layers. The boundaries between the two layers for the models with $Z = 0$ and $Z = 0.02$ are $3 \times 10^9 \text{ cm}$ and $8 \times 10^8 \text{ cm}$, respectively.

The parameter ranges of the outflow are as follows; (1) We adopt $L_{j,52}^{\text{iso}} = L_j^{\text{iso}}/(10^{52} \text{ erg s}^{-1}) = (4, 10)$ because the GRB isotropic luminosity is normally-distributed in the range of $L_\gamma^{\text{iso}} \sim 10^{51-54} \text{ erg s}^{-1}$ (Ghirlanda et al. 2010). (2) R_i corresponds to the size of central engine that is constrained by time variability of GRB prompt emission. Since an interval of the time variability Δt is of the order

of 10^{-3} s , R_i is presumed to be smaller than $c\Delta t \sim 10^8 \text{ cm}$. Therefore, we vary R_i for a range of $R_{i,7} = R_i/(10^7 \text{ cm}) = 1 \sim 10$. (3) σ_i is determined by the mechanism to launch relativistic jets. We construct models with $\sigma_i = 0$, which corresponds to the standard fireball model, and with a range of $\sigma_i = 0.1 \sim 10$, which corresponds to magnetized jet models. We note that the strength of magnetic field realizing adopted σ_i is $\sim 10^{12-15} \text{ Gauss}$ at R_i . (4) For the other parameters, we fix $\Gamma_{\text{max}} = 100$ referring to a requirement to avoid compactness problem (Piran 2004), and expediently set $\epsilon\Omega = 10^3 \text{ s}^{-1}$ assuming $\epsilon = 0.1$ and $\Omega = 10^4 \text{ s}^{-1}$. We note that $\epsilon\Omega$ is rather uncertain. Initial Lorentz factor of the outflow is fixed to be $\Gamma_i = 1.23$, which corresponds to the sound velocity of ultra-relativistic fluids $c_s = 1/\sqrt{3}$. We name the model with $(L_{j,52}^{\text{iso}}, Z) = (4, 0)$ Model A, $(L_{j,52}^{\text{iso}}, Z) = (10, 0)$ Model B, $(L_{j,52}^{\text{iso}}, Z) = (4, 0.02)$ Model C, and $(L_{j,52}^{\text{iso}}, Z) = (10, 0.02)$ Model D. The model parameters are summarized in Table 1.

In the two-dimensional relativistic hydrodynamics calculation, we set parameters of the relativistic jets corresponding to the parameters of GRB outflow. The relativistic jets are injected from the inner boundary at an enclosed mass $1.4M_\odot$ corresponding to a radius $R_{\text{in}} = 900 \text{ km}$. The initial half angle of jet is set to 15° (Zhang et al. 2003) and thus energy deposition rates of jets L_j is set to be $L_{j,51} = L_j/10^{51} \text{ erg s}^{-1} = 1.5$ and 3.4 , which give $L_{j,52}^{\text{iso}} = 4$ and 10 , respectively. We employ the Lorentz factor of the jet at the inner boundary as $\Gamma = 2.5$ by reference to § 3.2 and the energy density of the jet as to accelerate the jet to $\Gamma = 100$.

3. RESULTS

3.1. Initial composition

Figures 1a and 1b show the falling regions of the models. The matter at the intersection between the circumference of the falling region and the jet axis is located at the inner boundary when the jet injection initiates. In the models with $Z = 0$ (Model A and B), the jet injection initiates at early time for the model with $L_{j,52}^{\text{iso}} = 10$ (Model B), while it has to wait until the large portion of the material in the O layer falls in the model with $L_{j,52}^{\text{iso}} = 4$ (Model A) because the ram pressure of the jets cannot overcome that of the falling matter in the O layer (see Maeda & Tominaga 2009). As a result, the falling region of the model with $L_{j,52}^{\text{iso}} = 4$ is more extended than that of the model with $L_{j,52}^{\text{iso}} = 10$. On the other hand, in the models with $Z = 0.02$ (Model C and D), due to the low-density O layer the jet injections in both of the models with $L_{j,52}^{\text{iso}} = 4$ and 10 initiate at similar epochs and thus their falling regions are similar. The initial composition of the GRB outflow is derived from the integration of matter at the filled region because the matter at the shaded region is likely to be accreted to the central remnant before the initiation of the jet injection.

The composition of a mass element falling to $r = R_i$ depends on the maximum temperature that is higher for smaller R_i and for the matter locating initially at the in-

Table 1. Summary of the model parameters

Model	L_j^{iso} (10^{52} erg s $^{-1}$)	L_j (10^{51} erg s $^{-1}$)	Z	Γ_{max}	Γ_i	$\epsilon\Omega$ (s $^{-1}$)
A	4	1.5	0	100	1.23	10^3
B	10	3.4	0	100	1.23	10^3
C	4	1.5	0.02	100	1.23	10^3
D	10	3.4	0.02	100	1.23	10^3

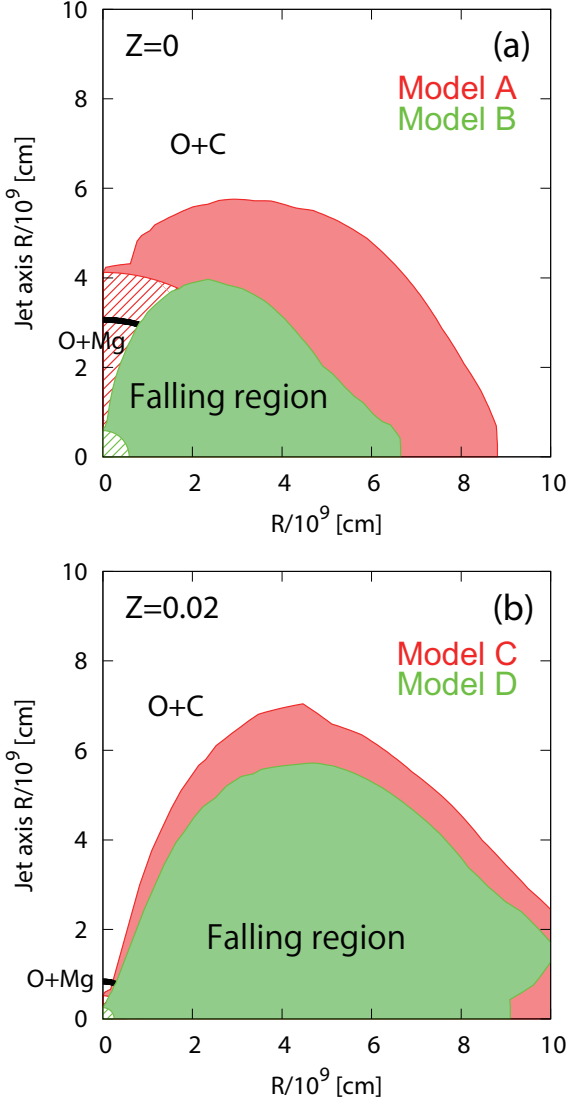


Fig. 1. Initial locations of the falling mass elements (filled and shaded regions), for (a) $Z = 0$ models (Model A and B) and (b) $Z = 0.02$ models (Model C and D). The shaded and filled regions represent the mass elements fell before and after the initiation of the jet injection, respectively. We assume that the outflow consists of the materials initially at the filled regions. The color of the regions represent the models with $L_{j,52}^{\text{iso}} = 4$ (green) and $L_{j,52}^{\text{iso}} = 10$ (red) and the background circles represent the boundaries between an inner O+Mg layer with $X(^{24}\text{Mg}) > X(^{12}\text{C})$ and an outer O+C layer with $X(^{24}\text{Mg}) \leq X(^{12}\text{C})$.

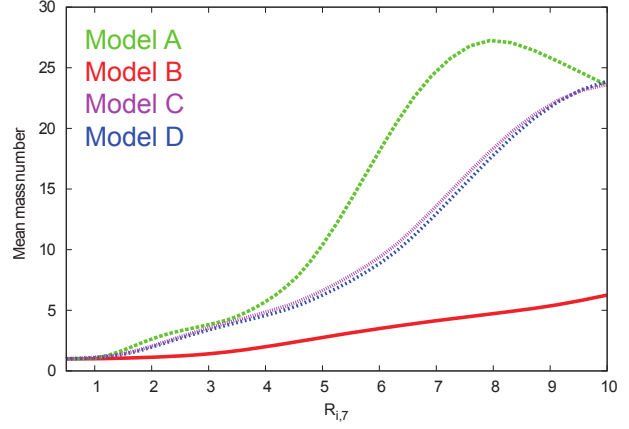


Fig. 2. Mean mass number of initial composition of the outflow.

ner layers. The mean mass numbers $\langle A \rangle$ of the initial composition of the outflow are shown as a function of R_i in Figure 2. The Model B has small $\langle A \rangle = 1 - 6$ for $R_{i,7} = 1 - 10$ because the jets consist of the matter initially locating in the inner layer, while the Model A can have $\langle A \rangle \geq 15$ for $R_{i,7} \geq 5.5$ because the heavy nuclei can survive in the outer matter that falls to the outer R_i . The most abundant nucleus in the models with $\langle A \rangle \geq 15$ is ^{28}Si due to the O burning during the fallback. The turnover at $R_{i,7} \sim 8$ stems from the fact that the maximum temperature of the mass elements in the outer layer is not high enough to ignite ^{16}O .

On the other hand, the jet injection in the models with $Z = 0.02$ (Model C and D) are initiated at early time and the outflow contains the matter initially locating in the O+Mg layer. The falling region are similar in both models and thus resultant $\langle A \rangle$ of the models are similar. In the models with $Z = 0.02$, the presupernova temperature of the infalling matter is lower than in the models with $Z = 0$ due to the low-density O layer. Therefore, $\langle A \rangle \geq 15$ is realized at $R_i \geq 7.3$ and the most abundant nucleus is ^{28}Si in these models.

3.2. Outflow dynamics

Hydrodynamical properties of the outflow for the models with $(L_{j,52}^{\text{iso}}, R_{i,7}, \sigma_i) = (4, 6, 0)$ and $(4, 6, 3)$ are shown in Figures 3(a)-3(d).

Figures 3(a) and (b) show evolution of the Lorentz factor as functions of r and fluid proper time t_p which is calculated by an integration $t_p = \int_{R_i}^r 1/(v\Gamma)dr$, respectively.

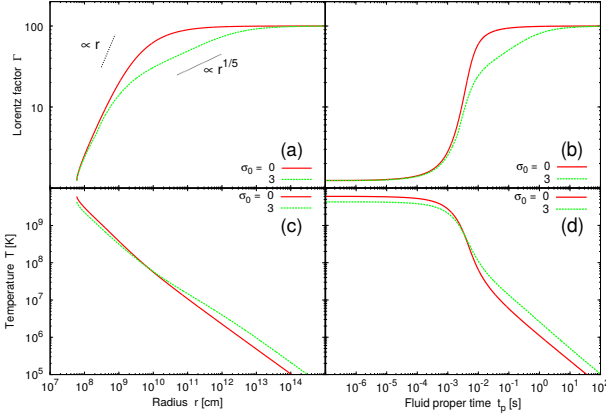


Fig. 3. Hydrodynamical properties of the models with $(L_{j,52}^{\text{iso}}, R_{i,7}, \sigma_i) = (4, 6, 0)$ and $(4, 6, 3)$: (a) radial evolution of Lorentz factor, (b) time evolution of Lorentz factor, (c) radial evolution of the temperature, and (d) time evolution of the temperature.

In the model with $\sigma_i = 0$, the Lorentz factor evolves linearly with radius until it reaches Γ_{max} as expected from the standard fireball model. The acceleration takes place at $t_p \sim 10^{-3} - 10^{-2}$ s. On the other hand, in the models with $\sigma_i = 3$, the outflow is accelerated initially by thermal pressure like the fireball model and later by magnetic field with the time scale of τ_{dis} . The Lorentz factor evolves more slowly than the model with $\sigma_i = 0$.

Figures 3 (c) and (d) show evolution of the temperature as functions of r and t_p , respectively. In the both models with $\sigma_i = 0$ and 3, the temperature decreases exponentially with t_p , during the phase in which the Lorentz factor evolves linearly with radius. This stems from the relations, $\Gamma \propto r$, $T \propto r^{-1}$, and $dt_p = dt/\Gamma \sim dr/c\Gamma$. While the temperature in the model with $\sigma_i = 3$ is lower than that in the model with $\sigma_i = 0$ before the acceleration, it decreases more slowly and becomes higher at $r > 10^{10}$ cm and $t_p > 10^{-2}$ s than in the model with $\sigma_i = 0$. This is because the acceleration is slow and the magnetic field energy is converted not only to the kinetic energy but also to the thermal energy in the model with $\sigma_i = 3$.

3.3. Nuclear composition

Figures 4 (a) and (b) show time evolution of nuclear composition of the outflow for models with $(L_{j,52}^{\text{iso}}, Z, R_{i,7}, \sigma_i) = (4, 0, 6, 0)$ and $(4, 0, 6, 3)$, respectively. Nuclear reaction ceases at $t_p \sim 10^{-2}$ sec in both models (a) and (b) because the temperature after the epoch falls below $\sim 10^8$ K (Figure 3d). The epoch corresponds to $r \simeq 10^{10}$ cm for the model with $(L_{j,52}^{\text{iso}}, Z, R_{i,7}, \sigma_i) = (4, 0, 6, 0)$ and $r \simeq 4 \times 10^9$ cm for the model with $(L_{j,52}^{\text{iso}}, Z, R_{i,7}, \sigma_i) = (4, 0, 6, 3)$.

In the model with $(L_{j,52}^{\text{iso}}, Z, R_{i,7}, \sigma_i) = (4, 0, 6, 0)$, which corresponds to the standard fireball model, heavy and intermediate mass nuclei are almost dissociated until $t_p \sim 10^{-5}$ s and ^4He and d are synthesized at $t_p > 10^{-3}$ s as the outflow cools. Only light nuclei and free nucleons, ^4He , d , p , and n , remain in the outflow after the acceleration

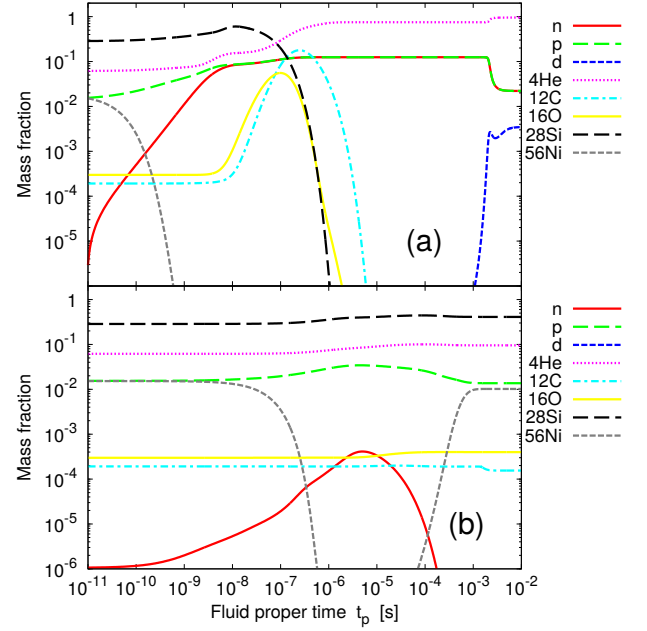


Fig. 4. Time evolution of nuclear composition for the models with (a) $(L_{j,52}^{\text{iso}}, Z, R_{i,7}, \sigma_i) = (4, 0, 6, 0)$ and (b) $(L_{j,52}^{\text{iso}}, Z, R_{i,7}, \sigma_i) = (4, 0, 6, 3)$.

(Figure 4a). This demonstrates that the standard fireball model with $(L_{j,52}^{\text{iso}}, Z, R_{i,7}, \sigma_i) = (4, 0, 6, 0)$ destroys heavy nuclei even if they are initially contained in the outflow.

On the other hand, in the model with $(L_{j,52}^{\text{iso}}, Z, R_{i,7}, \sigma_i) = (4, 0, 6, 3)$, whereas some nuclei such as ^{56}Ni are dissociated at $t_p < 10^{-6}$ s and re-synthesized at $t_p > 10^{-3}$ s, other nuclei such as ^{28}Si survive without dissociation and remain abundant after acceleration (Figure 4b). This illustrates that the metal nuclei can survive in the magnetized jet.

Figures 5(a)-5(d) show mean mass number of final nuclear composition as functions of R_i and σ_i for the model A, B, C, and D (see Table 1).

When a condition

$$T_9 > 3.6 \left(\frac{0.04}{t_p} \right)^{\frac{1}{33.3}} \quad (9)$$

is satisfied, quasi-statistical equilibrium (QSE) is attained (e.g., Woosley et al. 1973). The white solid line in Figures 5(a)-5(d) represents the criterion to establish QSE. Therefore, in the models with lower σ_i and smaller R_i than the white solid line, the composition can be described by QSE and the metal nuclei are almost destroyed due to the high entropy. This criterion is well fitted by a contour of initial temperature $T_{i,9} = T_i/10^9 \text{ K} = 4.7$ (green dotted line in Figure 5). On the other hand, as long as QSE is not attained, the models with larger R_i yield final compositions with heavier mean mass number except for the model B that initially does not have heavy nuclei (Figure 2).

Table 2 shows the 10 most abundant nuclei and their mass fractions for the model A, B, C, and D with $(R_i, \sigma_i) = (10, 10)$. In the model A, C, and D, ^{28}Si is most

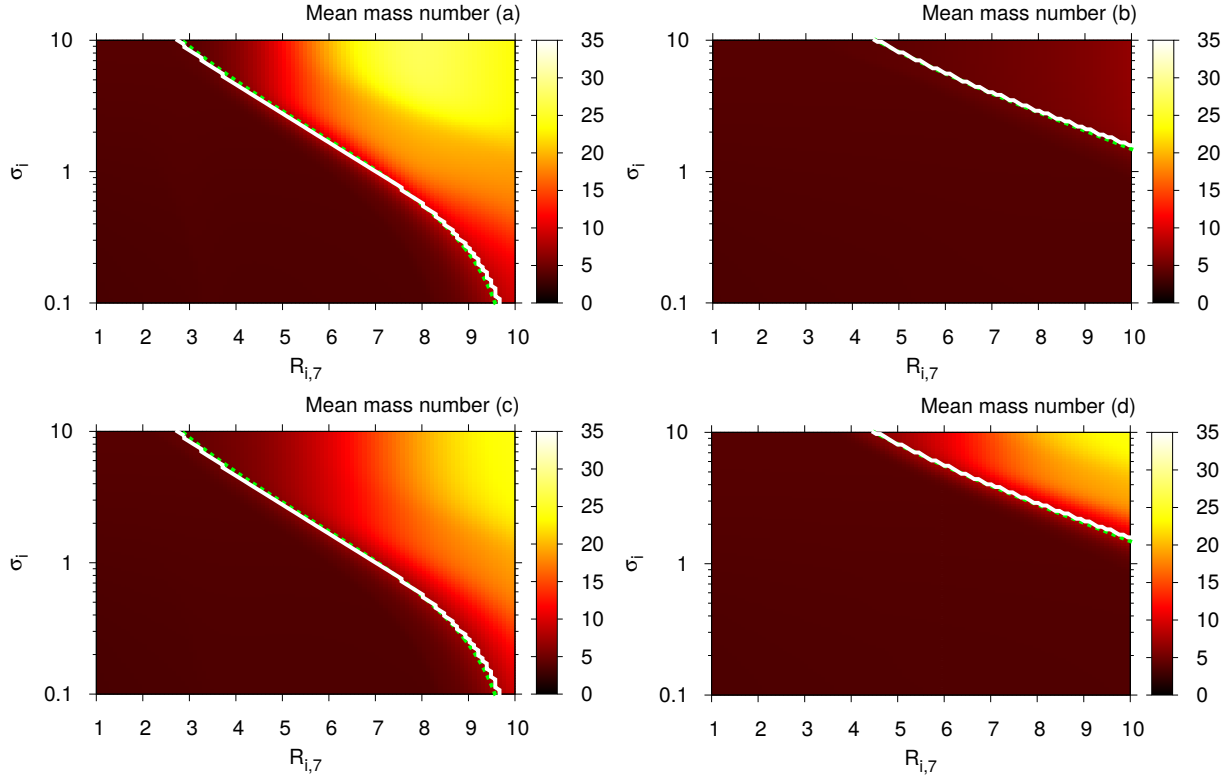


Fig. 5. Mean mass number of the final nuclear composition in the outflow as functions of R_i and σ_i for (a) model A, (b) model B, (c) model C, and (d) model D. The model parameters are summarized in Table 1. The white solid lines and green dotted lines represent the criterion for the QSE establishment and the contour of $T_{i,9} = 4.7$, respectively.

Table 2. The 10 most abundant nuclei and their mass fractions for the models A, B, C, and D with $(R_i, \sigma_i) = (10, 10)$.

	Model A		Model B		Model C		Model D	
1	^{28}Si ...	3.7182E-01	^4He ...	5.1509E-01	^{28}Si ...	3.9266E-01	^{28}Si ...	3.8889E-01
2	^{16}O ...	2.9626E-01	^{58}Ni ...	9.0864E-02	^{16}O ...	2.0150E-01	^{32}S ...	1.7979E-01
3	^{32}S ...	2.0439E-01	^{32}S ...	7.2190E-02	^{32}S ...	1.7598E-01	^{16}O ...	1.6323E-01
4	^{36}Ar ...	5.3067E-02	^{28}Si ...	5.8950E-02	^{54}Fe ...	6.9657E-02	^{54}Fe ...	8.7961E-02
5	^{40}Ca ...	4.1669E-02	^{54}Fe ...	5.7403E-02	^{36}Ar ...	3.9364E-02	^{36}Ar ...	4.0427E-02
6	^{54}Fe ...	1.0189E-02	^{55}Co ...	3.3212E-02	^{40}Ca ...	2.2114E-02	^{40}Ca ...	2.4969E-02
7	^{24}Mg ...	7.1779E-03	^{36}Ar ...	2.4232E-02	^{55}Co ...	1.6240E-02	^{55}Co ...	1.9738E-02
8	^{56}Ni ...	2.8607E-03	^{57}Ni ...	1.9790E-02	^{24}Mg ...	1.0641E-02	^{56}Ni ...	1.4527E-02
9	^{55}Co ...	2.1998E-03	^{16}O ...	1.8796E-02	^{58}Ni ...	8.9718E-03	^{58}Ni ...	1.3446E-02
10	^{58}Ni ...	1.2994E-03	^{56}Ni ...	1.4453E-02	^{56}Ni ...	8.8717E-03	^4He ...	1.0203E-02

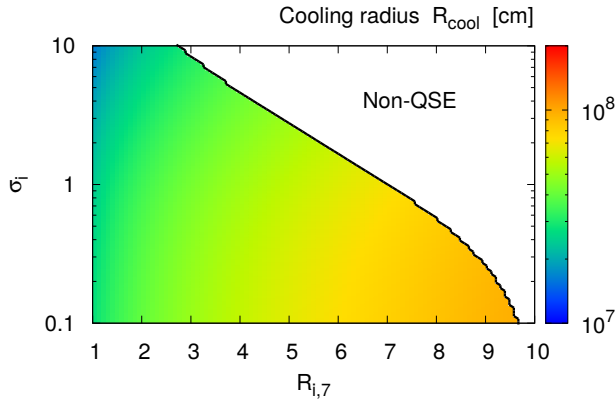


Fig. 6. The cooling radius R_{cool} , above which QSE is no longer established, as functions of R_i and σ_i for the model A.

abundant and its mass fraction reaches $\sim 40\%$. The mass fractions of ^{16}O and ^{32}S are also high in the model A, C, and D. In particular, the mass fraction of ^{16}O reaches $\sim 30\%$ in the models A. On the other hand, in the model B, the most abundant nucleus is ^4He the mass fraction of which is about $\sim 52\%$ and the mass fractions of each metal nucleus are less than 10% .

So far, we fix the isotropic jet luminosity as $L_{j,52}^{\text{iso}} = 4$ and 10 referring to canonical GRB isotropic luminosity. However, there are GRBs belonging to less energetic class called low-luminosity GRBs (LLGRBs) with $L_j^{\text{iso}} \lesssim 10^{49} \text{ erg s}^{-1}$ (e.g., Liang et al. 2007). From Equation (4) and the equation of state, the isotropic luminosity L_j^{iso} of a GRB jet is related to the initial temperature through e_{int} with Equation (1) as $L_j^{\text{iso}} \simeq 16\pi R_i^2 e_{\text{int}} \Gamma_i^2 v_i (1 + \sigma_i)/3$. Applying the condition for T_i to avoid the QSE establishment (i.e., $T_{i,9} < 4.7$), the condition in terms of the isotropic luminosity is obtained as follows,

$$L_j^{\text{iso}} \lesssim 3.9 \times 10^{50} R_{i,7}^2 (1 + \sigma_i) \text{ erg s}^{-1}. \quad (10)$$

According to this condition, the metal nuclei can be involved in the jets of the LLGRBs even within the framework of standard fireball model (i.e., $\sigma_i = 0$).

Figure 6 shows the cooling radius R_{cool} above which the condition to establish QSE is no longer satisfied; $R_{\text{cool}} \sim 10^{7-8} \text{ cm}$ depending on R_i and σ_i . Since QSE is not attained at $r > R_{\text{cool}}$, the metal nuclei, that have not been dissociated at $r \sim R_{\text{cool}}$, can survive after the acceleration. Furthermore, if the metal nuclei mix from the stellar mantle at $r > R_{\text{cool}}$, as discussed in Horiuchi et al. (2012), they are involved in the outflow without serious dissociation.

4. CONCLUSION

In this paper, we investigated nuclear composition of GRB jets assuming that the jets initially possess metal nuclei. We calculated fallback in a relativistic jet-induced explosion with a two-dimensional relativistic hydrodynamics calculation and derived the initial composition of the jet. Then, we calculated the acceleration of magnetized GRB

jets and detail nuclear reactions in the jets with the initial compositions.

We found that the composition of the falling matter after the jet injection depends on the radius to which the matter falls off and thus the initial composition of the jet depends on the size of the central engine of the jet. If the size of the central engine is larger than $R_{i,7} \gtrsim 5$, the matter contains metal nuclei abundantly except for the model with $Z = 0$ and $L_{j,52}^{\text{iso}} = 10$ (model B). Model B involves only a small fraction of metal nuclei with the mean mass number of $\langle A \rangle \leq 6$ even for $R_{i,7} \gtrsim 5$ because the jets consist of mass elements with high temperature in the presupernova star.

We conclude that the metal nuclei can survive in the jet if QSE is not established. The metal nuclei are dissociated mostly to ^4He once QSE is established. This is due to the high entropy of the jet being accelerated to $\Gamma = 100$, in which α -rich freezeout takes place. Therefore, the final nuclear composition of the jet is dominated by ^4He for the QSE-established models. The criterion for QSE establishment is well fitted by the contour of $T_{i,9} = 4.7$. The criterion leads to the condition of the isotropic jet luminosity L_j^{iso} as $L_j^{\text{iso}} \lesssim 3.9 \times 10^{50} R_{i,7}^2 (1 + \sigma_i) \text{ erg s}^{-1}$ and this is consistent with the results of Horiuchi et al. (2012) since the beaming correction for the jet reduces L_j^{iso} by the orders of ~ 2 .

The most popular model for acceleration of GRB jet is the fireball model, in which thermal pressure accelerates the jet from sub-relativistic to ultra-relativistic (Goodman 1986; Paczyński 1986; Mészáros 2006). In such the standard fireball model, $R_{i,7} > 5$ is required for the metal nuclei to survive in the jet with $L_{j,52}^{\text{iso}} \gtrsim 1$. If the jet has a luminosity of $L_{j,52}^{\text{iso}} \gtrsim 4$, the size of the central engine must be larger than 10^8 cm for the survival of metal nuclei. However, this violates a constraint on the size of central engine from time variability of the flux, i.e. $R_{i,7} \lesssim 10$. Therefore, at least, metal nuclei initially contained in the GRB jet with $L_{j,52}^{\text{iso}} \gtrsim 4$ should be destroyed and the final nuclear composition is dominated by light nuclei and free nucleons within the framework of the standard fireball model.

On the other hand, the magnetized jet has been proposed to explain spectra of some GRBs. For example, Zhang & Pe'er (2009) suggests that GRB 080916C involves a magnetized jet because a thermal component, that should appear in the spectrum if the jet energy is initially dominated by thermal energy, was not detected. Also, Guiriec et al. (2011) reports that GRB 100724B exhibits typical non-thermal spectrum, called Band spectrum, with a significant thermal component and suggests that a highly magnetized jet can explain the feature, which is quite challenging for the standard fireball model. In such a magnetized jet, the energy is initially possessed by the magnetic field, and thus the condition for QSE is avoidable in the jet even with high luminosities like $L_{j,52}^{\text{iso}} \gtrsim 10$ with satisfying $R_{i,7} \lesssim 10$, although $R_{i,7} \gtrsim 5$ is required for metal nuclei to initially exist in the jet in our model.

5. DISCUSSION

In this paper, we constrain the size of the central engine with the time variability of the gamma-ray emission since it could reflect the time variability of the central engine, for example, in the internal shock model. However, the time variability of the gamma-ray emission may come from other factors. For examples, the order of ~ 1 s variability can arise from the interaction between the jet and the progenitor star (Morsony, Lazzati, & Begelman 2010), or the time variability may be related to the emission mechanism itself, e.g. turbulent motion at the gamma-ray emitting region (e.g., Zhang & Yang 2011). In these cases, the size of the central engine is not necessarily constrained, at least, by the time variability and the larger $R_{i,7} > 10$ is possible. If the size of the central engine is as large as $R_{i,7} = 50$, the criterion for the survival of the metal nuclei is $L_j^{\text{iso}} \lesssim 10^{53}(1 + \sigma_i) \text{ erg s}^{-1}$, indicating that a large fraction of GRBs can possess the metal nuclei in the jet even with $\sigma_i = 0$.

We treated the GRB jet as a steady, radial, magnetized outflow for simplicity. However, in reality, the jet should propagate through the progenitor and the interaction between them is expected. Such an interaction could affect the dynamics of the jet. For examples, it is suggested that the initial confinement by the collapsing stellar material has an important role on the collimation of magnetically dominated jets from magnetars (Uzdensky & Macfadyen 2007). The cocoon, which is a shocked hot gas surrounding the jet, also have a role to collimate the jet (e.g., Morsony, Lazzati, & Begelman 2007; Mizuta & Aloy 2009; Bromberg et al. 2011). If the jet is collimated, the evolution of jet cross section $\Sigma(r)$ may be expressed as $\Sigma(r) \propto r^\xi$ with $\xi < 2$. In this case, the temperature, and also the density, will decrease slowly than in the radial flow and the criterion, Equation (10), possibly tighten because the fluid will tend to keep the high temperature at the initial stage.

Metzger, Giannios, & Horiuchi (2011) investigated the nucleosynthesis from free nucleons in the magnetically dominated jet in the context of the protomagnetar model for the central engine of GRBs (Metzger et al. 2011). The main difference between their work and this paper is the parameter range of the entropy per baryon. They estimated the entropy per baryon in the jet with the analytic expression derived in Qian & Woosley (1996) for the neutrino-driven winds. They suggested that, since the entropy per baryon in the neutrino driven wind is sufficiently low, the heavy nuclei beyond the iron peak, i.e., $A \gtrsim 56$ where A is a mass number, can be synthesized in the jet. On the other hand, we do not consider such sufficiently low entropy environment for synthesis of metal nuclei from free nucleons and we focus only on the survival of the metal nuclei in this paper. Future studies on the central engine of GRBs will reveal whether such low entropy environment is realized or not.

It is known that GRBs are one of the candidates for the origin of ultra high energy cosmic rays (UHECRs) (e.g., Waxman 1995; Vietri 1995) and LLGRBs are also possible

candidates for the origin of UHECRs (e.g., Murase et al. 2006; Gupta & Zhang 2007). The acceleration of metal nuclei up to ultra-high energies could be possible in both usual high-luminosity GRBs and LLGRBs (Wang et al. 2008; Murase et al. 2008). Abraham et al. (2010) reported that the observed UHECRs are dominated by heavy nuclei at high energies, i.e., $E \gtrsim 10^{19}$ eV (see, however, Abbassi et al. 2010). Hooper & Taylor (2010) suggested that the result of Abraham et al. (2010) can be quantitatively reproduced only if UHECR composition at the accelerating site mainly consist of intermediate mass nuclei such as nitrogen together with a considerable fraction of heavy nuclei such as iron. Therefore, GRBs with magnetized jets or LLGRBs have a potential to be the origin of UHECRs in terms of, at least, the nuclear composition because intermediate mass nuclei, e.g. ^{28}Si , are very abundant in the jet. However, in order to explore whether the model considered in this paper can quantitatively explain the UHECR observations, acceleration process, escape from the source, and the propagation of the UHE nuclei from the source to the Earth also have to be considered. Such calculations are beyond the scope of this paper and will be studied elsewhere.

Acknowledgments

We thank Hajime Susa for his helpful comments. This research has been supported in part by World Premier International Research Center Initiative, MEXT, Japan, and by the Grant-in-Aid for Scientific Research of the JSPS (23740157, 25-2912). Data analyses were in part carried out on the general-purpose PC farm at the Center for Computational Astrophysics, CfCA, of National Astronomical Observatory of Japan.

References

- Abbasi, R. U., et al. 2010, *Phys. Rev. Lett.*, 104, 161101
- Abraham, J., et al. 2010, *Phys. Rev. Lett.*, 104, 091101
- Beloborodov, A. M. 2003, *ApJ*, 588, 931
- Bisnovatyi-Kogan, G. S., 2002, *Stellar Physics. Vol.2: Stellar Evolution and Stability*, (Berlin: Springer)
- Blandford, R. D., & Znajek, R. L. 1977, *MNRAS*, 179, 433
- Bromberg, O., Nakar, E., Piran, T., & Sari, R., *ApJ*, 740, 100
- Brown, G. E., Lee, C.-H., Wijers, R. A. M. J., Lee, H. K., Israelian G., & Bethe, H. A. 2000, *New A*, 5, 191
- Drenkhahn, G. 2002, *A&A*, 387, 714
- Drenkhahn, G., & Spruit, H. C. 2002, *A&A*, 391, 1141
- Freiburghaus, C., Rembges, J.-F., Rauscher, T., Kolbe, E., Thielemann, F. K., Kratz, K.-L., Pfeiffer, B., & Cowan, J. J. 1999, *ApJ*, 516, 381
- Fryer, C. L. 1999, *ApJ*, 522, 413
- Fryer, C. L., & Mészáros, P. 2003, *ApJ*, 588, L25
- Fujimoto, S., Nishimura, N., & Hashimoto, M. 2008, *ApJ*, 680, 1350
- Ghirlanda, G., Nava, L., & Ghisellini, G. 2010, *A&A*, 511, 43
- Goodman, J. 1986, *ApJL*, 308, L47
- Guiriec, S., et al. 2011, *ApJL*, 727, L33
- Gupta, N., & Zhang, B., 2007, *Astroparticle Physics*, 27, 386
- Hix, W. R., & Thielemann, F.-K. 1996, *ApJ*, 460, 869
- Hix, W. R., & Thielemann, F.-K. 1999, *ApJ*, 511, 862

- Hooper, D., & Taylor, A. M. 2010, *Astropart. Phys.*, 33, 151
- Horiuchi, S., Murase, K., Ioka, K., & Mészáros, P. 2012, *ApJ*, 753, 69
- Iwamoto, K., et al. 1998, *Nature*, 395, 672
- Lemoine, M. 2002, *A&A*, 390, L31
- Liang, E., Zhang, B., Virgili, F., & Dai, Z. G. 2007, *ApJ*, 662, 1111
- Lyutikov, M., & Blandford, R. D. 2003, *arXiv:astro-ph/0312347*
- Maeda, K., & Nomoto, K. 2003, *ApJ*, 598, 1163
- Maeda, K., & Tominaga, N. 2009, *MNRAS*, 394, 1317
- MacFadyen, A. I., & Woosley, S. E. 1999, *ApJ*, 524, 262
- McKinney, J. C. 2006, *MNRAS*, 368, 1561
- Mészáros, P. 2006, *Rep. Prog. Phys.*, 69, 2259
- Metzger, B. D., Giannios, D., Thompson, T. A., Bucciantini, N., & Quataert, E., 2011, *MNRAS*, 413, 2031
- Metzger, B. D., Giannios, D., & Horiuchi, S., *MNRAS*, 415, 2495
- Mizuta, A., & Aloy, M. A., 2009, *ApJ*, 699, 1261
- Morsony, B. J., Lazzati, D., & Begelman, M. C., 2007, *ApJ*, 665, 569
- Morsony, B. J., Lazzati, D., & Begelman, M. C., 2010, *ApJ*, 723, 267
- Murase, K., Ioka, K., Nagataki, S., & Nakamura, T. 2006, *ApJ*, 651, L5
- Murase, K., Ioka, K., Nagataki, S., & Nakamura, T. 2008, *Phys. Rev. D*, 78, 023005
- Paczynski, B. 1986, *ApJL*, 308, L43
- Piran, T. 2004, *Rev. Mod. Phys.*, 76, 1143
- Pruet, J., Guiles, S., & Fuller, G. M. 2002, *ApJ*, 580, 368
- Qian, Y. -Z., & Woosley, S. E., 1996, *ApJ*, 471, 331
- Saio, H., Nomoto, K., & Kato, M. 1988, *ApJ*, 331, 388
- Tominaga, N., Maeda, K., Umeda, H., Nomoto, K., Tanaka, M., Iwamoto, N., Suzuki, T., & Mazzali, P. A. 2007, *ApJ*, 657, L77
- Tominaga, N. 2009, *ApJ*, 690, 526
- Umeda, H., & Nomoto, K. 2005, *ApJ*, 619, 427
- Uzdensky, D. A., & Macfadyen, A. I., 2007, *ApJ*, 669, 546
- Vietri, M. 1995, *ApJ*, 453, 883
- Wang, X. Y., Razzaque, S., & Mészáros, P. 2008, *ApJ*, 677, 432
- Waxman, E. 1995, *Phys. Rev. Lett.*, 75, 386
- Woosley, S. E. 1993, *ApJ*, 405, 273
- Woosley, S. E., Arnett, W. D., & Clayton, D. D. 1973, *ApJS*, 26, 231
- Zhang, B., & Pe'er, A. 2009, *ApJ*, 700, L65
- Zhang, W., Woosley, S. E., & Macfadyen, A. I. 2003, *ApJ*, 586, 356
- Zhang, B., & Yan, H., 2011, *ApJ*, 726, 90